Diurnal Variations of the Martian Surface Layer Meteorological Parameters During the First 45 Sols at Two Viking Lander Sites[1]

JORDAN L. SUTTON, CONWAY B. LEOVY AND JAMES E. TILLMAN

Department of Atmospheric Sciences, University of Washington, Seattle 98195

(Manuscript received 19 October 1977, in final form 5 September 1978)

ABSTRACT

Wind speed, ambient and surface temperatures from both Viking Landers have been used to compute bulk Richardson numbers and Monin-Obukhov lengths during the earliest phase of the Mars missions. These parameters are used to estimate drag and heat transfer coefficients, friction velocities and surface heat fluxes at the two sites. The principal uncertainty is in the specification of the roughness length. Maximum heat fluxes occur near local noon at both sites, and are estimated to be in the range 15–20 W m^{-2} at the Viking 1 site and 10–15 W m^{-2} at the Viking 2 site. Maximum values of friction velocity occur in late morning at Viking 1 and are estimated to be 0.4–0.6 m s^{-1}. They occur shortly after dawn at the Viking 2 site where peak values are estimated to be in the range 0.25–0.35 m s^{-1}. Extension of these calculations to later times during the mission will require allowance for dust opacity effects in the estimation of surface temperature and in the correction of radiation errors of the Viking 2 temperature sensor.

1. Introduction

The acquisition of meteorological data from the surface of Mars by the two Viking Landers makes it possible for the first time to estimate atmospheric boundary layer parameters for another planet. The landers touched down near midsummer at two Northern Hemisphere sites: 47°W, 23°N for Viking 1 (VL-1) and 227°W, 48°N for Viking 2 (VL-2). Martian seasons are conveniently referenced to the longitude L_s of the sun in Mars-centered coordinates (aerocentric longitude), with $L_s=0$ corresponding to northern spring equinox. In this paper, we estimate boundary layer parameters for the first 45 sols at each site (the *sol* is the Martian day, equivalent to 24 h, 39 min, 35 s), with L_s extending from 98° to 120° at VL-1 and from 120° to 143° at VL-2. The meteorological data for these periods have been described by Hess *et al.*, (1976a,b, 1977).

The boundary layer parameters are estimated by the bulk aerodynamic method (Priestley, 1959). That is, the wind speed at the measurement level is combined with the difference between the measured atmospheric temperature and the ground surface temperature to determine a bulk Richardson number. The bulk Richardson number is then related to Monin–Obukhov length using flux-gradient relationships obtained from terrestrial boundary layer experiments. Finally, drag and heat transfer coefficients and momentum and heat fluxes are estimated with the aid of the computed Monin–Obukhov lengths. The ground surface temperature required in this approach is obtained from a thermal model, described by Kieffer (1976), based on measurements by the Viking Orbiter Infrared Thermal Mappers (IRTM). The surface roughness length z_0 is a parameter in the calculations, and we have at this stage in our analysis no independent estimates of this quantity beyond visual inspection of the Viking Lander images of the surface. Consequently, calculations have been carried out for two extreme values of z_0 which we believe bound the range of probable values. Fortunately, the results are not excessively sensitive to this parameter. Additional results are presented for a boundary layer model which incorporates a molecular heat conduction layer near the surface.

2. Data

The meteorological measurement system has been described in detail by Chamberlain *et al.* (1976). Only the wind speed and temperature measurements are used here. Wind speed is measured by a pair of hot-film sensors which are orthogonal to each other in the plane of the lander footpads and which operate at a nearly constant overheat. The actual overheat and the power required to maintain it are measured. The plane of the lander footpads is tilted slightly with respect to the horizontal, especially at lander 2, but these tilts are small enough to have negligible effect on the horizontal wind speed measurements. The sensors were calibrated before flight, and their performance at Mars is checked by comparison with a "wind quadrant sensor", which consists of thermocouples arranged around a heated

[1] Contribution No. 438, Department of Atmospheric Sciences, University of Washington.

0022-4928/78/2346-2355$05.00

vertical cylinder. Although this device was designed primarily to provide wind direction information, it also provides an independent solution for wind speed when operating in the wind speed range of the measurements described here. In practice a solution for wind speed and wind direction is obtained by combining the redundant data from the hot-film and wind quadrant sensors by minimizing the least-square residuals for wind speed and direction. The resulting standard deviation of the wind speed solution provides a check on the total system performance. Two sensors measure atmospheric temperature: 1) the primary sensor is a thermocouple array mounted out of the flow from the hot film sensors; 2) the secondary sensor is a resistance thermometer, mounted between the wind sensors, whose main purpose is to provide the reference temperature for controlling the wind sensor overheats. The entire assembly is mounted on a boom 1.6 m above the ground and 0.8 m away from the nearest point of the lander body. When the sensors are not in the lander plume, the wind speed errors are estimated to be about $\pm 10\%$ and the absolute temperature errors ± 1.5°C (Hess *et al.*, 1977). Temperature errors at the VL-2 site are slightly greater than this because of failure of the primary temperature sensor on that lander so that the secondary sensor, subject to significant radiation and conduction errors, had to be relied on. Although we believe these errors have been limited to approximately the ± 2°C level during the first 45 sols, extension of atmospheric temperatures to later periods will require further processing of the VL-2 data. It is partly for this reason that our analysis is restricted to this early part of the mission.

The spacecraft computer dumps 16 discrete data samples at a time, and the averages of each 16-sample group, which we shall call the "dump-averages", provided the basic data set. The sampling interval and the length and timing of the dumps were controlled by the onboard computer system to values which could be set by ground command. Values were picked to insure adequate sampling of diurnal variations, adequate sampling for fluctuations of different frequencies, and to minimize the loss of data due to other spacecraft activities. The data dumps analyzed here include sampling frequencies ranging from 1 s^{-1} to 1/64 s^{-1}. Because of limitations on the total data return and interference with other spacecraft activities, sampling was not generally continuous, and the possibility for unrepresentative sampling exists. In order to reduce the influence of unrepresentative sampling as well as random errors in the measurements, the dump-average data were averaged further and then smoothed over the diurnal cycle using the following procedure.

1) Dump averages with mean wind directions known to be influenced by lander interference were eliminated from the data. Based on prelaunch testing and observed effects in the temperature measurements, lander interference was assumed to occur when dump average wind directions were in the range 246–33° for VL-1 and 126–212° for VL-2. Lander interference was most important during the morning hours for VL-2 and was almost completely absent for VL-1. When present, its primary effect was to introduce spurious temperature errors of up to +8°C, and it may also have produced wind speed reductions of up to about 10%.

2) Dump averages for periods of 15 sols each for each lander were grouped into 25 diurnal bins to yield three "composite sols" of 25 equally spaced bins for each of the three groups of 15 sols for each lander. Care was taken to avoid biased temperatures within bins due to uneven sampling of the rapid daily temperature variations.

3) The composite sol data were smoothed by means of a least-squares fifth-order harmonic fit. The daily wind and temperature patterns obtained in this way closely resemble those given by Hess *et al.* (1976a,b, 1977), differing slightly in the periods covered, and in the removal of most lander interference effects in the present data.

TABLE 1. Ground temperature model parameters. Thermal inertia is the product of thermal conductivity and volumetric heat capacity of the soil.

Viking lander site	Albedo	Thermal inertia (W m^{-2} – K)	Solar declination (deg)
VL-1	0.260	272.1	22.83
VL-2	0.225	334.9	21.94

Kieffer has used Viking IRTM measurements obtained just before dawn and near midday to determine best-fit albedos and thermal inertias for the two sites under the assumptions that the soil is homogeneous and that skies are clear (Kieffer, 1976). There was a moderate amount of suspended atmospheric dust early in the Viking missions, but experimentation with the soil temperature model suggests that moderate opacities due to dust will not significantly affect the shape of the diurnal ground temperature curve, although albedo and thermal inertia estimates will be slightly biased. The ground temperatures were modeled with the best-fit thermal inertias and albedos given in Table 1. Only one solar declination, corresponding roughly to the midpoint of the entire 45-sol period, was used for each site. Although it is difficult to judge the overall accuracy of these homogeneous ground temperature models, the transition periods between stable and unstable conditions at the surface are easily identified from the character of the fluctuations of wind speed and atmospheric temperature. The latter, shown in Fig. 1b, coincide reasonably well with the changes in sign of the atmosphere-ground temperature difference inferred from the ground temperature models (Fig. 1a). Some significant departures from the homogeneous surface model have been found at locations in the latitude belt

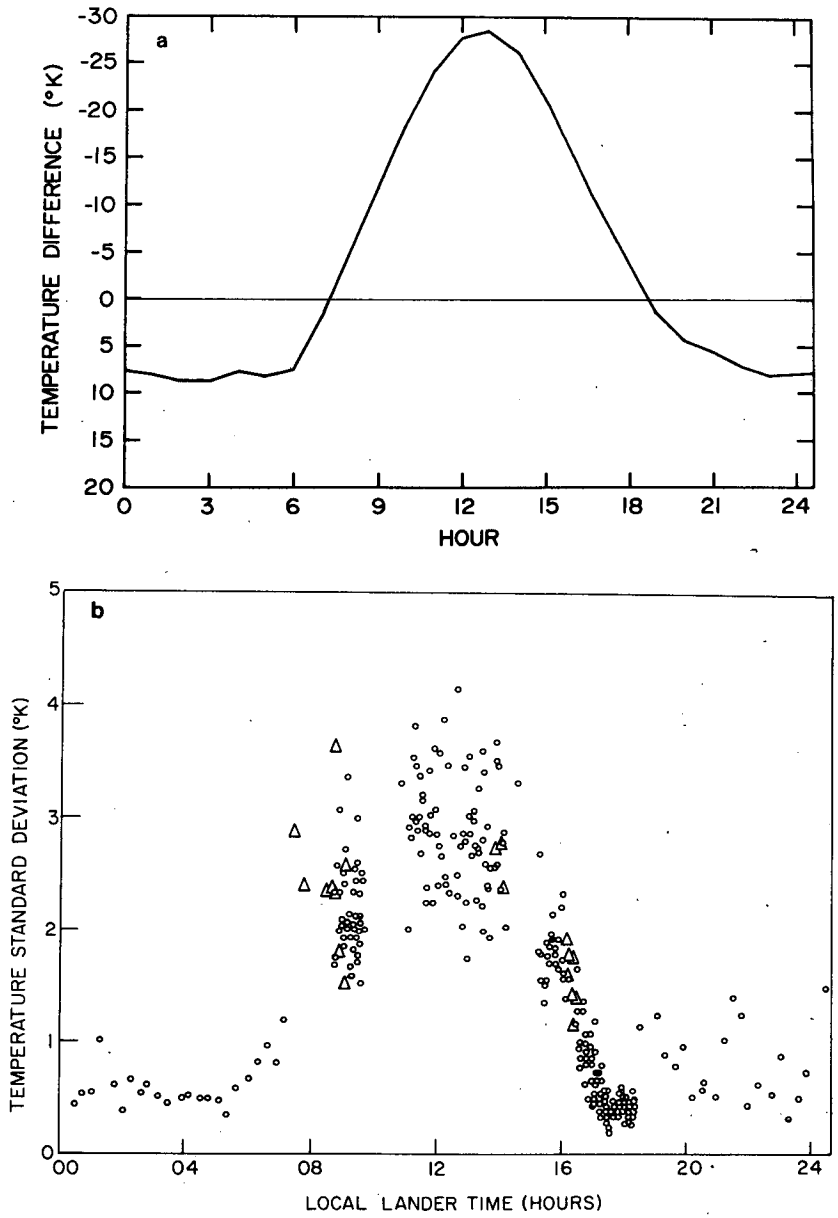

FIG. 1. (a) Atmosphere-ground temperature difference versus time in hours per sol, for VL-1 sols 31–45, based on the meteorology experiment atmospheric temperature and Kieffer's (1976) ground temperature model. (b) Standard deviation of temperature within the 16-point data dumps for sol 35 at VL-1. Points shown by triangles correspond to dumps influenced by lander interference. The standard deviation increase between 1800 and 1900 is due in part to an increase in sampling interval from 4 to 64 s.

of the VL-2 site. At these locations, ground temperature falls below that predicted by the homogeneous surface model between 1400 and 1900 LT, with a discrepancy of as much as 10°C. Thus, heat fluxes during late afternoon may be overestimated as a result of this discrepancy, particularly at the VL-2 site. Nevertheless, the extreme values of the fluxes and their general trends should be approximated well with the use of these models.

The most uncertain quantity in these calculations is the roughness length z_0. It is not determined directly, but can be estimated using the Viking Lander images and the method suggested by Lettau (1969). These show rather homogeneous flat or gently undulating terrain generally covered with fine-grained material, but littered with rocks of varying size (Mutch *et al.*, 1976a,b). Typically, rocks in the near vicinity of the landers are about fist-sized, although there are numerous

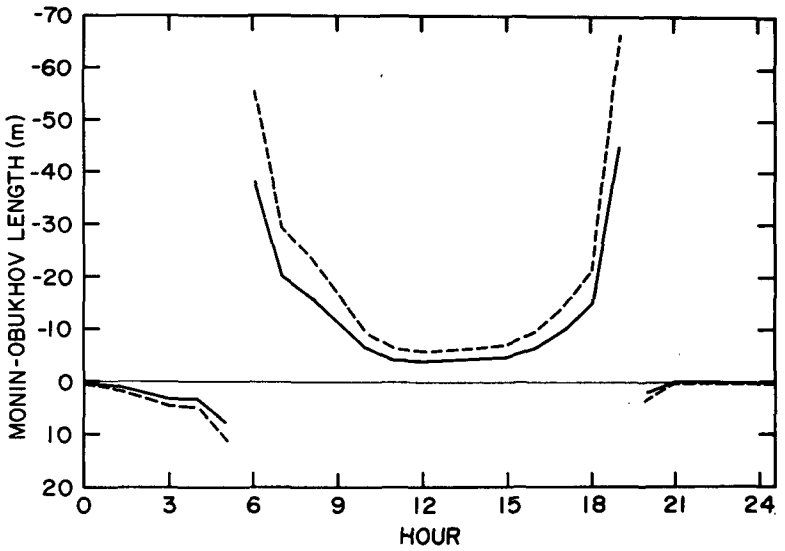

FIG. 2. Variation of the Monin-Obukhov length as a function of time for VL-2 sols 31–45. The solid line corresponds to $z_0=0.1$ cm, the dashed line to $z_0=1.0$ cm.

smaller and a few larger blocks. There is little or no azimuthal variability of the terrain characteristics at the VL-2 site, but at VL-1 there are some features which may cause some directional dependence of z_0. For example, the general rock-strewn terrain about the lander is broken to the northeast by dunes and some particularly large blocks. On this rather crude basis, we estimate that z_0 at both sites lies well within the range 0.1–1.0 cm and calculations are done for both of these cases in order to reasonably bound the possibilities.

3. Monin-Obukhov length, heat flux, and friction velocity

The meteorological data and ground temperature models provide estimates of wind speed u and atmosphere-ground potential temperature difference $\Delta\theta$ as functions of time of day for each 15-sol group at each site. From these, one can construct a bulk Richardson number

$$\mathrm{Ri_B}=\frac{gz\Delta\theta}{u^2\bar{T}}, \tag{1}$$

where $g=3.72$ m s^{-2} is Martian surface gravity, z the instrument height (1.61 m), and $\bar{T}$ the mean of the ground and atmosphere temperatures. $\mathrm{Ri_B}$ can be related to the Monin–Obukhov length,

$$L=-\frac{u_*^3\bar{T}c_p\rho}{kgH}, \tag{2}$$

where u_* is friction velocity, c_p specific heat at constant pressure, ρ the atmospheric density, k von Kármán's constant (0.4 in our calculations), and H the convective heat flux (positive upward). According to boundary layer similarity theory, the wind shear and temperature gradient are given by

$$\frac{du}{dz}=\frac{u_*}{kz}\phi_m(\zeta), \tag{3}$$

$$\frac{d\theta}{dz}=-\frac{H}{\rho c_p k u_* z}\phi_h(\zeta), \tag{4}$$

where ζ is the dimensionless height, $(=z/L)$ and ϕ_m and ϕ_h are functions which are now well known from experiments in the terrestrial boundary layer and which are assumed to be universal (e.g., Clarke, 1970). Integration of (3) and (4) between dimensionless heights $\zeta_0=z_0/L$ and ζ, and substitution into (1) yields

$$\mathrm{Ri_B}=\frac{gz\Delta\theta}{u^2\bar{T}}=\frac{\zeta\left[\int_{\zeta_0}^{\zeta}\zeta^{-1}\phi_h(\zeta)d\zeta\right]}{\left[\int_{\zeta_0}^{\zeta}\zeta^{-1}\phi_m(\zeta)d\zeta\right]^2}=f(z,z_0,L). \tag{5}$$

This procedure assumes that the atmospheric temperature is equal to the ground temperature at height z_0. Although this is a widely used assumption, we examine the implications of an alternative assumption below. We assume that ϕ_m and ϕ_h are truly universal functions of their argument, and apply the following relationships determined empirically for the earth (Businger *et al.*, 1971):

$$\left.\begin{aligned}\phi_m&=1+4.7\zeta\\ \phi_h&=0.74+4.7\zeta\end{aligned}\right\} \tag{6a}$$

for the statically stable boundary layer ($\zeta>0$, $\Delta\theta>0$) and

$$\left.\begin{aligned}\phi_m&=(1-15\zeta)^{-\frac{1}{4}}\\ \phi_h&=0.74(1-9\zeta)^{-\frac{1}{2}}\end{aligned}\right\} \tag{6b}$$

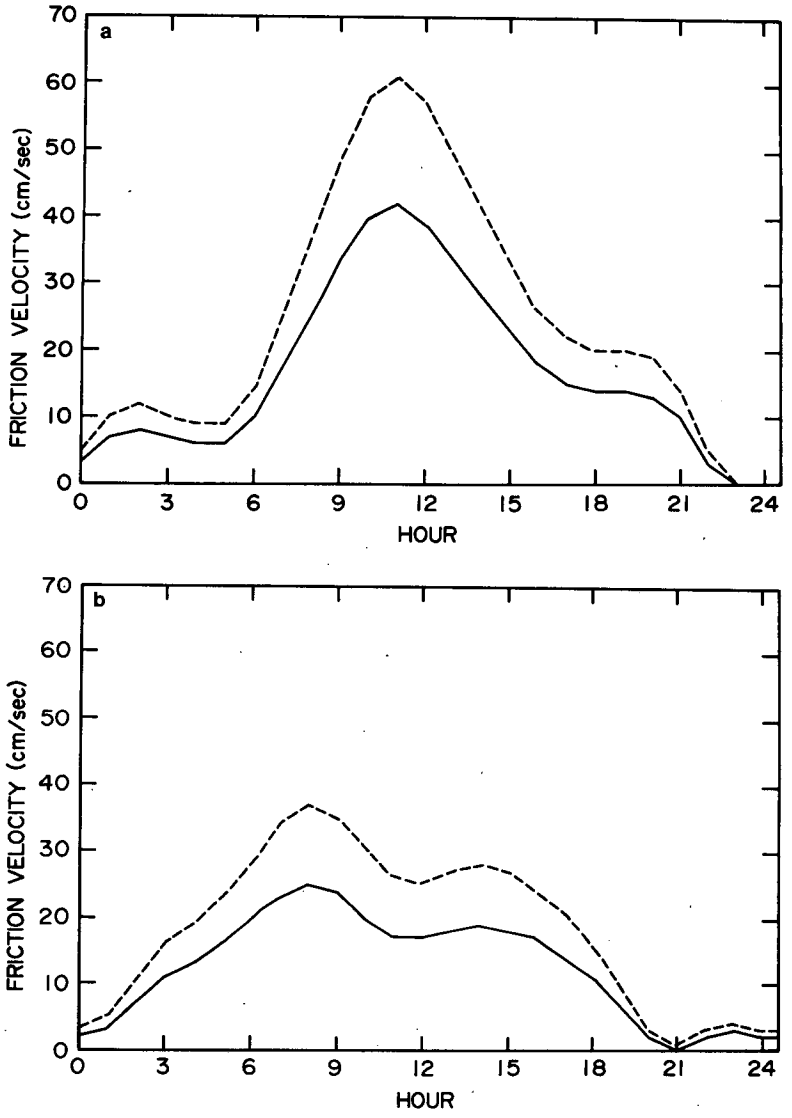

FIG. 3. Friction velocity for VL-1 sols 16–30 (a) and VL-2 sols 0–15 (b) for $z_0=0.1$ cm (solid) and 1.0 cm (dashed).

for the unstable boundary layer ($\zeta<0$, $\Delta\theta<0$). When z and z_0 are fixed, the right side of Eq. (5) is a monotonic function of L, except for extremely stable cases when the critical bulk Richardson number for the extinction of turbulence is exceeded ($\mathrm{Ri_B}>1/4.7$). Then no valid solution to (5) exists. Thus, except for the few cases of supercritical bulk Richardson number, L can be found for any observed value of $\mathrm{Ri_B}$ by a simple computer search procedure. Results of this process are illustrated in Fig. 2. This shows the familiar hyperbolic behavior of L. It is small and negative during the highly unstable midday and early afternoon period, and small and positive during the extremely stable periods at night when the wind is also very light. It has positive and negative infinities at the times of stability transition. Cases of supercritical bulk Richardson number are shown as zero values of L in this figure.

Integration of (3) and (4) also yields expressions for u_* and H in terms of u and $\Delta\theta$:

$$u_*=C_d(\zeta,\zeta_0)u, \tag{7}$$

$$H=-\rho C_p u_* C_h(\zeta,\zeta_0)\Delta\theta, \tag{8}$$

where the drag coefficient C_d is given by

$$C_d(\zeta,\zeta_0)=k\left[\int_{\zeta_0}^{\zeta}\zeta^{-1}\phi_m(\zeta)d\zeta\right]^{-1}, \tag{9}$$

and the heat transfer coefficient C_h is given by

$$C_h(\zeta,\zeta_0)=k\left[\int_{\zeta_0}^{\zeta}\zeta^{-1}\phi_h(\zeta)d\zeta\right]^{-1}. \tag{10}$$

Fig. 3a shows friction velocity calculated in this way for the VL-1 site for sols 16–30 for the two assumed

values $z_0=0.1$ cm (solid curve) and $z_0=1.0$ cm (dashed curve). The variations arise from two effects: the wind speed variation, which exhibits a late morning maximum, and the stability variation as reflected in the variation of the Monin–Obukhov length. Thus, there is a marked late morning peak with very low values at night. Zero values correspond to supercritical Richardson numbers, when the flow becomes laminar. Fig. 3b is a similar plot for the VL-2 site. It differs from the VL-1 site in having generally lower wind speeds, especially during the afternoon, and less instability so that u_* values are smaller, but otherwise the features are similar to those at the VL-1 site. Curves for the other 15-sol periods are very similar and are not given here. Figs. 4a and 4b display the corresponding heat fluxes. Here the influence of stability is greater; it enters both in the Monin–Obukhov length and in the factor $\Delta\theta$ in Eq. (8). Consequently, heat flux is very sharply peaked at noon. Note also that heat flux is relatively sensitive to z_0 under the assumption that the atmosphere and ground temperatures are equal at height z_0.

4. Calculations with a molecular thermal sublayer

The assumption that atmosphere and ground temperatures are equal at height z_0 is likely to be a poor one at best, and especially so on Mars. Molecular kinematic viscosity and thermal diffusivity coefficients are two orders of magnitude larger there than on Earth because of the low atmospheric density, and one can anticipate that molecular sublayers at the surface will

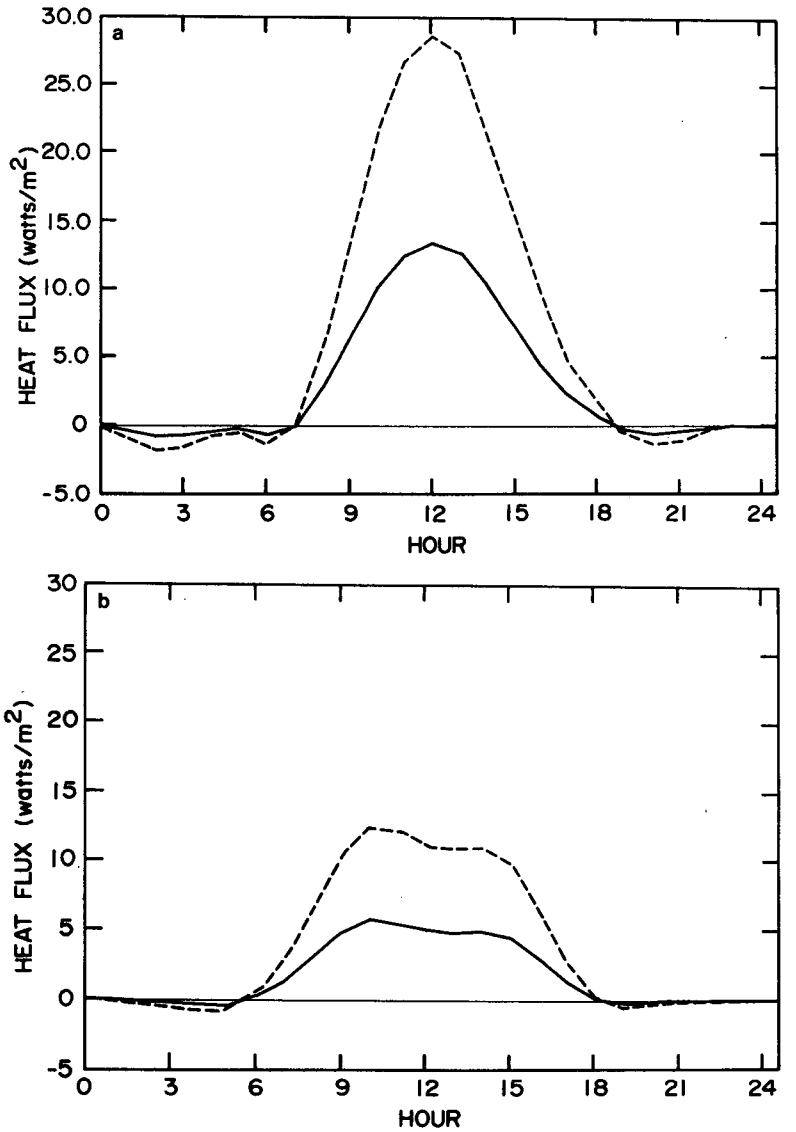

FIG. 4. Heat flux for VL-1 sols 16–30 (a) and VL-2 sols 0–15 (b) for $z_0=0.1$ cm (solid) and 1.0 cm (dashed).

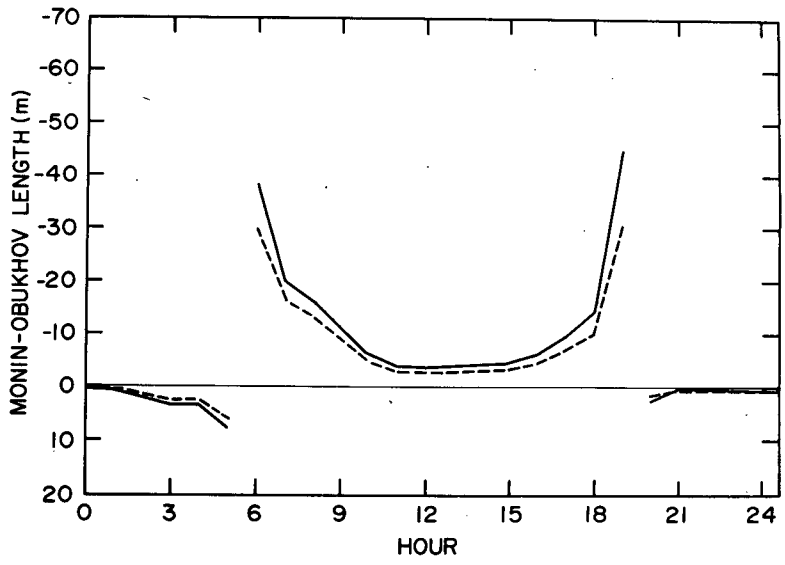

FIG. 5. Monin-Obukhov length for VL-1 sols 16–30 when the molecular heat conduction sublayer is taken into account.

be more in evidence. With our assumed roughness lengths, aerodynamically rough or quasi-rough surface flow should prevail during most daytime hours, with a comparatively smooth flow at night at both sites. We have estimated the correction to the drag coefficient for these nighttime cases, and find the maximum effect at night amounting to about a 20% correction to the rough flow drag coefficients. Since momentum and heat fluxes are very small at night, detailed calculations have not been carried out for smooth surface flow. The influence of a molecular heat conduction layer can be more significant, however, and, following a suggestion of Leovy (1969), calculations have been performed assuming a heat conduction sublayer at all times of day. In this model, a sharp transition between molecular and turbulent heat transfer is assumed to occur at height $z_*=\kappa/ku_*$, where κ is the molecular thermal diffusivity ($\sim 10^{-3}$ m^2 s^{-1} at the surface of Mars). With this assumption, the temperature drop across the boundary layer is given by

$$\Delta\theta=-\frac{H}{\rho C_p k u_*}\left[1+\int_{\zeta_*}^{\zeta}\zeta^{-1}\phi_h(\zeta)d\zeta\right],$$

where $\zeta_*=z_*/L$. Eq. (5) is replaced by

$$\mathrm{Ri_B}=\frac{gz\Delta\theta}{u^2\bar{T}}=\frac{\zeta\left[1+\int_{\zeta_*}^{\zeta}\zeta^{-1}\phi_h(\zeta)d\zeta\right]}{\left[\int_{\zeta_0}^{\zeta}\zeta^{-1}\phi_m(\zeta)d\zeta\right]^2}=f_*(z,z_*,z_0,L), \quad (5^*)$$

while

$$C_h(\zeta,\zeta_*)=k\left[1+\int_{\zeta_*}^{\zeta}\zeta^{-1}\phi_h(\zeta)d\zeta\right]^{-1}. \quad (10^*)$$

In Eq. (5*), z is known and z_0 is assumed; z_* and L are both unknowns. Thus it was necessary to obtain the solution iteratively by evaluating (5*), (7) and (9) for each assumed value of L. Convergence of the iterations is rapid however. A slightly more complex but self-consistent procedure which would have eliminated the need to assume z_0 values would have been to assume an analogous transition between viscous and turbulent momentum boundary layers at height $z_s=\nu/ku_*$, where ν is the kinematic viscosity. In view of the probable occurrence of relatively rough flow during daytime, and the rather small differences in u_* values which were obtained by assuming rough or smooth flows, we chose not to use this procedure.

Fig. 5 shows the Monin–Obukhov length for this model corresponding to the same case as that displayed in Fig. 2. The qualitative behavior of L is unchanged. Friction velocities derived from this model are also little different from those shown in Fig. 3. Heat fluxes are noticeably different, however, and are illustrated in Figs. 6a and 6b. The principal effect of this modeling assumption is to reduce the influence of z_0 on the heat fluxes. We believe that the heat fluxes shown in Figs. 6a and 6b are a better indication of the true situation than are those shown in Figs. 4a and b.

5. Discussion

The diurnal behavior of the wind speed and the atmosphere-ground temperature difference on Mars is very similar to that occurring in terrestrial deserts. Consequently, the computed boundary layer parameters L, u_* and H also behave in a similar fashion. Errors in the estimated values of u_* and H may arise from four sources: 1) errors in ground temperature, 2) errors in measured atmospheric temperature, 3) errors in measured values of wind speed and 4) errors due to the boundary layer model with its use of empirical relationships based on terrestrial boundary layer experiments

and assumed rather than measured values of z_0. The first two error sources would influence the results primarily through an absolute shift in $\Delta\theta$, either in Eq. (8) or in the analogous equation for the molecular thermal sublayer model. The contribution of the ground temperature uncertainty to total error in $\Delta\theta$ is much larger than the contribution of error in measured atmospheric temperature.

Since the ground temperature model was fitted to data points obtained shortly before dawn and near local noon, the ground temperature is most reliable at these times of day when it is probably accurate to better than ± 5°C. Larger errors (up to 10°C) could occur at other times of day. It can be seen from Fig. 1a that such errors imply an error in midday values of $\Delta\theta$ and in the corresponding values of heat flux of order $\pm 20\%$, and an error in the predawn values of order $\pm 50\%$. It is fair to say that during the night only the sign and an upper limit on the magnitude of the heat flux have been determined. The calculations for different values of z_0 and for two different boundary conditions on temperature give an indication of the sensitivity of the results to boundary layer models and parameters, but it is obviously desirable to have an independent check on the results. The high-frequency fluctuations of temperature and wind speed provide one possible check, and as detailed processing of the Viking fluctuation data proceeds, one of us (J.E.T.) plans to apply the method of Tillman (1972) to this problem. At present we must rely on relatively crude comparisons. For example, during strongly unstable conditions, the standard deviation of the horizontal

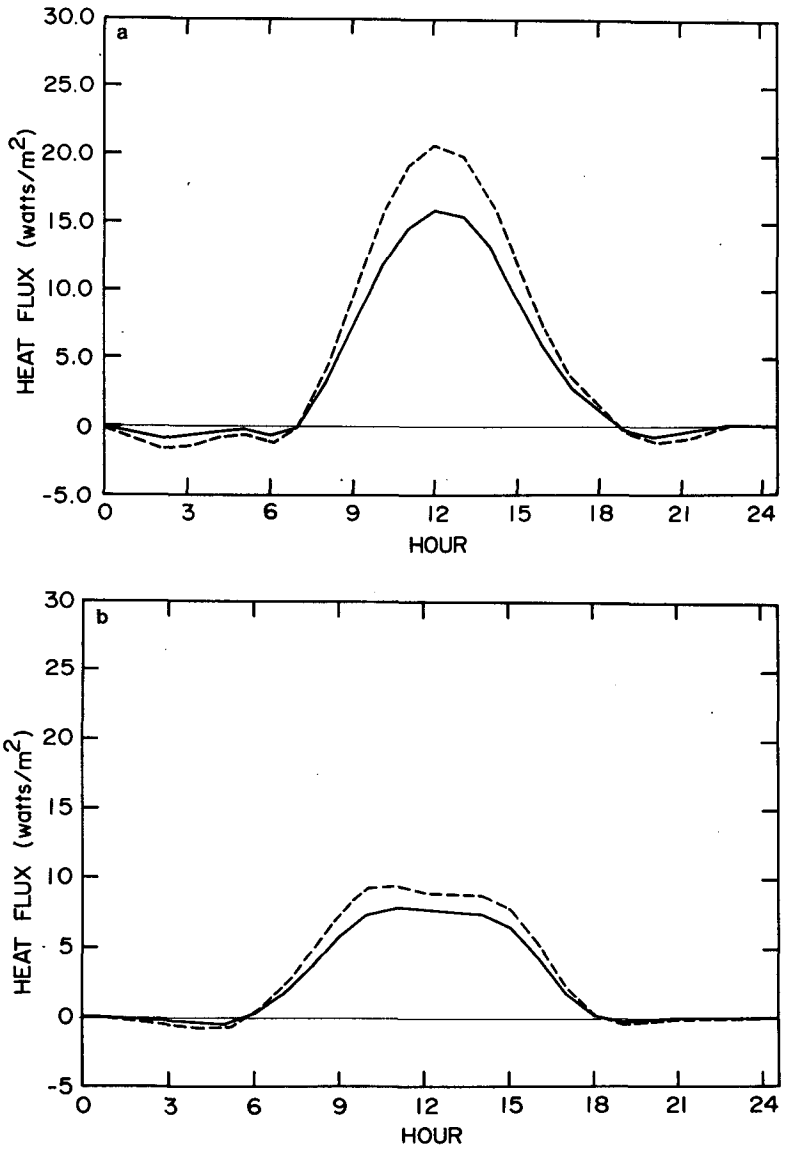

FIG. 6. As in Fig. 4 except the heat fluxes are obtained taking into account the molecular conduction sublayer.

wind velocity is approximately 0.5–0.6 of the bulk free convection velocity w_* where

$$w_* = (gHh/\rho C_p \bar{T})^{\frac{1}{3}}, \quad (11)$$

and h is the height of the convective boundary layer (Deardorff, 1972; Panofsky *et al.*, 1977). From the heights of the convective clouds observed in the Martian tropics by Briggs *et al.* (1977) and from the VL-1 entry temperature sounding (Seiff and Kirk, 1977), we infer that the daytime convective boundary layer at VL-1 is of order 4 km deep. For a 4 km layer with surface heat flux 15 W m^{-2}, convective velocity of about 3.7 m s^{-1} is inferred and the corresponding wind speed standard deviation 2.3 m s^{-1}. This compares with peak observed values of wind speed standard deviation at VL-1 of about 2.5 m s^{-1} (Hess *et al.*, 1977).

One can also use the temperature variance to obtain a quite independent estimate of heat flux. Under free convection conditions, heat flux is given by $H/\rho c_p = 1.08[\sigma_T{}^3 kgz/\bar{T}]^{\frac{1}{2}}$, where $\sigma_T{}^2$ is the temperature variance (e.g., Wyngaard *et al.*, 1971; Tillman, 1972). Substituting $\sigma_T \approx 3$°C corresponding to midday conditions (Fig. 1b), one obtains $H \approx 10$ W m^{-2}. The $|L|$ values are low enough to place the noon Viking measurements in the free-convection regime, and we conclude from the agreement of this estimate with the heat flux deduced by the bulk aerodynamic method that the latter is not grossly in error. Note that each method of estimating H incorporates some spatial averaging. The bulk aerodynamic method uses a ground temperature representative of the region within about 10 km of the lander and a time (and hence upwind) averaged gas temperature. The methods based on standard deviation of wind or temperature rely on time-averaged, and hence upwind-averaged statistics.

If the heat fluxes shown in Figs. 6a and 6b are correct, the total daily convective heat input would be sufficient to warm a layer 5 km deep by an average of 7°C sol^{-1}. Five kilometers is likely to be the characteristic maximum depth of the Martian diurnal convective boundary layer, based on the VL-1 entry temperature profile and the orbiter imaging observations of convective clouds. A maximum convective boundary layer depth of 6–8 km was obtained in a numerical simulation of the Martian general circulation (Pollack *et al.*, 1976), but the model did not allow for absorption of solar radiation by suspended dust, the effect of which is to stabilize the atmosphere and suppress the boundary layer (Pollack *et al.*, 1978). A boundary layer 4 or 5 km deep during midafternoon would be deeper by about a factor of 2 than typical terrestrial diurnal convective boundary layers formed under desert conditions during midsummer. We can also compare the relative magnitudes of Martian and terrestrial heat fluxes. The midday convective heat flux on Mars appears to reach about 2% of the available solar flux. This can be compared with peak heat fluxes in terrestrial deserts of about 20% of the available solar flux. Taking into account the differences in the solar fluxes at the two planets, we obtain a peak Martian convective flux per unit atmospheric mass of about three times its terrestrial counterpart. Thus, we infer that the convective boundary layer on Mars is only moderately more active than that of terrestrial deserts. There is no evidence for lower atmosphere mixing rates as large as those used in some photochemical models (e.g., McElroy and Kong, 1976). In contrast, there is direct evidence for high mixing rates in the photochemically critical 40–60 km altitude region (Anderson and Leovy, 1978).

Values of u_* are of particular interest from the point of view of the minimum surface stress required to produce saltation of grains. Laboratory experiments extrapolated to Martian conditions suggest that the minimum value of u_* required to initiate saltation is near 2.5 m s^{-1} and occurs for sand-sized particles, those with radii of order 300 μm (Greeley *et al.*, 1976). During the light wind regime of the early Viking mission, all estimated u_* values are much less than this. However, stronger winds have been observed later in the mission. The strongest winds were observed shortly after the onset of the second of two planetwide dust storms at the VL-1 site. A substantial wind speed of 17.7 m s^{-1} was reached with peak gust of 27.6 m s^{-1}. Such strong winds would insure an essentially neutral boundary layer, so that $C_d \approx k[\ln(z/z_0)]^{-1}$. One can then estimate that u_* was probably in the range 1–2 m s^{-1} depending on the roughness length. Thus measured winds at the landing sites do not appear to have reached the saltation threshold even during periods when the planet was generally obscured by dust storm activity. The threshold value of 2.5 m s^{-1} depends on particle cohesion, and would be lower if the cohesion were less than that assumed by Greeley *et al.*, however. It will be of great interest to see whether detailed analysis of the Viking lander images reveals any evidence for grain motion near the VL-1 lander.

During later phases of the mission, the atmospheric opacity due to dust reached very large values (Pollack *et al.*, 1977, 1978). This would have a strong influence on both the modeled ground temperatures and on the radiation correction for the Viking 2 temperature sensor. Thus, extension of the heat flux calculations by means of the bulk aerodynamic method to later times during the mission must await detailed evaluation of the radiative effects of the suspended dust.

Acknowledgments. We are indebted to the many individuals who have made analysis of the Viking meteorological measurements possible, particularly to T. E. Chamberlain for engineering support, to W. Simon, R. G. Dutton, and W. Underwood for data processing support, and R. M. Henry for his continued close attention to the Viking data. Donn Terry also

assisted us in processing the Viking meteorology data tapes. Hugh Kieffer has generously made his results available and provided valuable comments on an earlier version of the manuscript. James Deardorff and Seymour Hess have made helpful comments about the Viking data as boundary layer measurements. This work was supported in part by the National Aeronautics and Space Administration under Grant NASI-9464.

REFERENCES

Anderson, E., and C. B. Leovy, 1978: Mariner 9 television limb observations of dust and ice hazes on Mars. *J. Atmos. Sci.*, **35**, 723–734.

Briggs, G. A., K. Klaasen, T. Thorpe, J. Wellman and W. Baum, 1977: Martian dynamical phenomena during June–November, 1976, Viking Orbiter imaging results. *J. Geophys. Res.*, **82**, 4121–4150.

Businger, J. A., J. C. Wyngaard, Y. Izumi and E. F. Bradley, 1971: Flux-profile relationships on the atmospheric surface layer. *J. Atmos. Sci.*, **28**, 181–189.

Chamberlain, T. E., H. L. Cole, R. G. Dutton, G. C. Greene and J. E. Tillman, 1976: Atmospheric measurements on Mars: The Viking meteorology experiment. *Bull. Amer. Meteor. Soc.*, **57**, 1094–1104.

Clarke, R. H., 1970: Recommended methods for the treatment of the boundary layer in numerical models. *Aust. Meteor. Mag.*, **18**, 51–73.

Deardorff, James W., 1972: Numerical investigation of neutral and unstable planetary boundary layers. *J. Atmos. Sci.*, **29**, 91–115.

Greeley, R., B. White, R. Leach, J. Iverson and J. Pollack, 1976: Mars: Wind friction speeds for particle movement. *Geophys. Res. Lett.*, **3**, 417–420.

Hess, S. L., *et al.*, 1976a. Mars climatology from Viking 1 after 20 sols. *Science*, **194**, 78–81.

——, *et al.*, 1976b: Early meteorological results from the Viking 2 lander. *Science*, **194**, 1352–1353.

——, *et al.*, 1977: Meteorological results from the surface of Mars: Viking 1 and 2. *J. Geophys. Res.*, **82**, 4559–4574.

Kieffer, Hugh H., 1976: Soil and surface temperatures at the Viking landing sites. *Science*, **194**, 1344–1346.

Leovy, C. B., 1969: Bulk transfer coefficient for heat transfer. *J. Geophys. Res.*, **74**, 3313–3321.

Lettau, H., 1969: Note on aerodynamic roughness parameter estimation on the basis of roughness element description. *J. Appl. Meteor.*, **8**, 828–832.

McElroy, M. and T. Y. Kong, 1976: Oxidation of the Martian surface: Constraints due to chemical processes in the atmosphere. *Geophys. Res. Lett.*, **3**, 569–572.

Mutch, T. A., *et al.*, 1976a: The surface layer of Mars: the view from the Viking 2 lander. *Science*, **194**, 1277–1283.

——, *et al.*, 1976b: The surface of Mars; the view from the Viking 1 lander. *Science*, **193**, 791–800.

Panofsky, H. A., H. Tennekes, D. H. Lenschow and J. C. Wyngaard, 1977: The characteristics of turbulent velocity components in the surface layer under convective conditions. *Bound.-Layer Meteor.*, **11**, 355–362.

Pollack, J. B., C. B. Leovy, Y. Mintz and W. vanCamp, 1976: Winds on Mars during the Viking season: predictions based on a general circulation model with topography. *Geophys. Res. Lett.*, **3**, 479–482.

——, D. Colburn, R. Kahn, J. Hunter and W. vanCamp, C. E. Carlston and M. R. Wolfe, 1977: Properties of aerosols in the Martian atmosphere as inferred from Viking lander imaging data. *J. Geophys. Res.*, **82**, 4479–4496.

——, ——, F. M. Flasar, C. E. Carlston and D. Pidock, 1979: Properties and effects of dust particles suspended in the Martian atmosphere. *J. Geophys. Res.* (in press).

Priestley, C. H. B., 1959: *Turbulent Transfer in the Lower Atmosphere.* University of Chicago Press, 130 pp.

Seiff, A., and D. B. Kirk, 1977: Structure of the atmosphere of Mars in summer at mid-latitudes. *J. Geophys. Res.*, **82**, 4364–4378.

Tillman, J. E., 1972: The indirect determination of stability, heat, and momentum fluxes in the atmospheric boundary layer from simple scalar variables during dry unstable conditions. *J. Appl. Meteor.*, **11**, 783–792.

Wyngaard, J. C., O. R. Coté and Y. Izumi, 1971: Local free convection, similarity, and the budgets of shear stress and heat flux. *J. Atmos. Sci.*, **28**, 1171–1182.